

Nonlinear analysis of a riverine platform under earthquake and environmental loads

Ahmed Abdelraheem Farghaly^{*1} and Denise-Penelope N. Kontoni^{2a}

¹Department of Civil and Architectural Constructions, Faculty of Industrial Education, Sohag University, Sohag 82524, Egypt

²Department of Civil Engineering, Technological Educational Institute of Western Greece, 1 M. Alexandrou Str., Koukoulí, GR-26334 Patras, Greece

(Received September 18, 2017, Revised March 5, 2018, Accepted March 29, 2018)

Abstract. A realistic FEM structural model is developed to predict the behavior, load transfer, force distribution and performance of a riverine platform under earthquake and environmental loads. The interaction between the transfer plate and the piles supporting the platform is investigated. Transfer plate structures have the ability to redistribute the loads from the superstructure above to piles group below, to provide safe transits of loads to piles group and thus to the soil, without failure of soil or structural elements. The distribution of piles affects the distribution of stress on both soil and platform. A materially nonlinear earthquake response spectrum analysis was performed on this riverine platform subjected to earthquake and environmental loads. A fixed connection between the piles and the platform is better in the design of the piles and the prospect of piles collapse is low while a hinged connection makes the prospect of damage high because of the larger displacements. A fixed connection between the piles and the platform is the most demanding case in the design of the platform slab (transfer plate) because of the high stress values developed.

Keywords: riverine platform; pile group foundation; soil-pile interaction; earthquake loads; environmental loads; materially nonlinear analysis; response spectrum analysis; FEM

1. Introduction

The Nile river water pump station at the Western project in the first Shush Street was investigated to assess the safety of the structure under earthquake, environmental, working and own weight loads. The river platform subject to dead, live, earthquake and environmental loads (wind, wave, and current loads), is a marriage between the flat plate and the piles. The plate transfers the loads to the piles and the piles transfer the loads to the soil surrounding and under the piles.

Kaynia (2012) studied the effect of flexible slabs on the dynamic and seismic responses of pile groups. Tallavó *et al.* (1995) studied the average frequency of a platform. Chau *et al.* (2009) studied the nonlinear seismic soil-pile-structure interactions of a model on a shaking table. Hamilton (2014) studied pile-soil interactions in unsaturated soil conditions. Asgarian *et al.* (2012) studied the effect of soil pile structure interaction on the dynamic characteristics of jacket type offshore platforms. Kaynia and Andersen (2015) and Kaynia *et al.* (2015) represent the soil under a platform as springs for the dynamic analysis of platforms. Hussien *et al.* (2010) studied the seismic response of end bearing piles supporting simple structures. Lysmer and Kuhlemeyer

(1969) concluded that the maximum deflection in the

upper part of the pile decreases with pile depth, and an increase of pile size did not cause a significant impact on pile response. Kim *et al.* (2015) studied a laterally loaded mono-pile type offshore wind turbine supported by a series of discrete springs, each having its own nonlinear load-displacement characteristics. Yi *et al.* (2015) studied wind turbine offshore models considering pile-soil-interaction. Cheng and Lui (2012) studied the reliability analysis of steel cable-stayed bridges including soil-pile-interaction. Dode *et al.* (2014) studied a building supported on pile groups. Abu Seif and El-Shater (2010) concluded that Sohag Governorate, especially in floodplain region, has encountered construction problems because of its sedimentation history and deep foundations are usually used to reduce settlement. Durante *et al.* (2015) investigated the complex seismic pile-soil interaction phenomenon by testing models on a shaking table. Ravi Kumar Reddy and Gunneswara Rao (2011) studied experimentally and numerically the model of a building frame supported by pile groups embedded in cohesionless soil. Chore *et al.* (2010) concluded that the increase in the piles numbers in a group decreases the displacement, the increase in the pile diameter reduces the displacement, parallel configuration of pile group yields higher displacement than the series arrangement, end bearing piles yield less displacement than floating piles, and the SSI is found to increase the maximum negative and positive bending moment on piles. Razavi *et al.* (2007) recommended avoiding the use of batter piles with plumb piles in a design. Chatterjee *et al.* (2015) studied the seismic behavior of a laterally loaded

*Corresponding author, Associate Professor
E-mail: khodary20002000@yahoo.com

^a Associate Professor
E-mail: kontoni@teiwest.gr



Fig. 1 Platform View

pile applying a pseudo-static methodology. Mehndiratta *et al.* (2014) found that the decrease of the piles' diameter, increase the response of the pile groups. Mandal *et al.* (2012) investigated the lateral load carrying capacity of a short pile in layered soil. Abdel-Mohti and Khodair (2014) studied the pile-soil interaction in a soft soil under lateral loading using the finite difference and finite element software which defined soil as isolated springs. Ukritchon *et al.* (2016) concluded that the maximum effect happens at the corner piles of a pile group and it decreases as the location of the pile gets closer to the center but increases again below the applied vertical load. Additional detailed discussion on SSI can be found in the book by Elnashai and Di Sarno (2015).

In this paper, a 3D FEM model of an existing riverine offshore platform supported by a piles group with special distribution was analyzed under earthquake and environmental loads (wind, wave, and current loads). A realistic model of the full scale model was developed from different structural elements (piles and platform) with its real specification and represents the soil as spring-gap elements at the interaction between the bed level soil and the piles, while under the bed level as spring-dashpot elements at the interactions between the piles and the soil, with different soil layers through which the piles pass. The effects of the earthquake loads and the different kinds of environmental loads on the platform were investigated, which confirmed that there are probable failures to occur in the platform and the piles carrying it, while the soil surrounding the piles suffers from separation.

2. Model description

The pump station consists of a pedestrian bridge with a length of 90 m mounted on 62 piles and a pile-supported platform with dimensions of 26 m x 17 m as shown in Fig. 1. The transfer reinforced concrete plate of the platform is 800 mm thick with upper and lower reinforcement meshes $8\phi 18/m'$ in both directions, rebar chairs $\phi 22/m'$ in both directions and reinforcement cover 50 mm at top and

bottom. The platform plate is mounted on 108 piles (with circular section of 550 mm diameter with steel pipe casing thickness 20 mm) 25 m length (14 m embedded in the river bed) away from the river bank by 100 m. The dead and live loads acting on the platform are: steel frame = 300 KN, six pumps = 600 KN, two generators = 60 KN, electricity panel = 5 KN, live load = 10 KN/m². The steel frame and the equipment loads on the deck were modeled as distributed load on the platform. Table 1 represents the geometrical and material properties for the elements of the platform and pile group foundation; these values of E_C and μ_C are also used by Chore and Ingle (2008). Fig. 2 shows the dimensions and the arrangement of piles in the platform.

2.1 Computer modeling of the platform

A three-dimensional structural model was constructed by the finite element method and materially nonlinear response spectrum analysis was performed. Two models with fixed and hinged connection between the piles and the platform were compared. The SAP2000 v.17 computer program was used to estimate the response of the transfer plate and the pile group. The plate is modeled using thick shell elements. All piles were modeled utilizing frame elements.

Table 1 Geometrical and material properties for the elements of the platform and pile group foundation

Properties	Corresponding Values
Pile diameter (D)	550 mm
Length of pile (L)	25 m
Thickness of pile cap	800 mm
Grade of concrete used for pile cap	Characteristic compressive strength: 40 MPa
Young's modulus of elasticity (E_C)	0.3605×10^8 KPa
Poisson's ratio for concrete (μ_C)	0.15

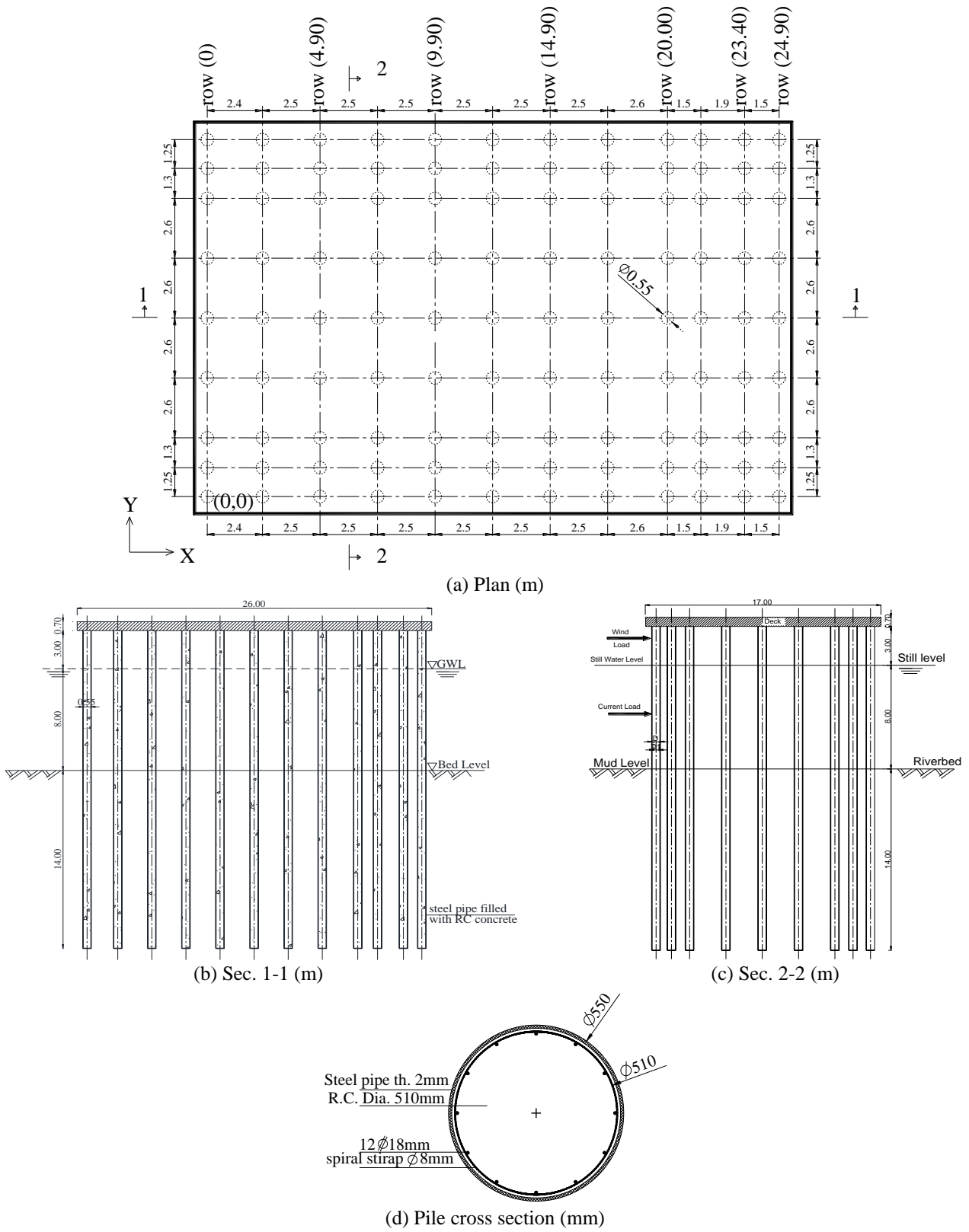


Fig. 2 A platform sections and plans

The soil (until 2 m depth) was modeled by spring-gap elements (Fig. 3) with stiffness k and gap distance δ used between each pile and the soil at a depth of 1 m under the soil surface both in x and y directions, to account for the gap that may occur between the pile and soil due to the lateral load actions. For the remaining depth (under the 2 m), the soil was modeled by soil springs (without gap) in three-dimensions until the bearing level (i.e., the end) of each pile. The soil around the pile group was considered to be formed of three layers with different properties.

The 3D finite element model of the platform used in SAP2000 v.17 is shown in Fig. 4.

2.2 Applied loads

The platform subjected to the following loads:

- Own weight of the steel frame structure, the RC plate, weight of the equipment and moving loads of the forklift, and live load on the RC plate.
- Environmental loads consisting of wind, wave and current loads.

Earthquake loads.



Fig. 3 The spring-gap element (at 1 m under bed level)

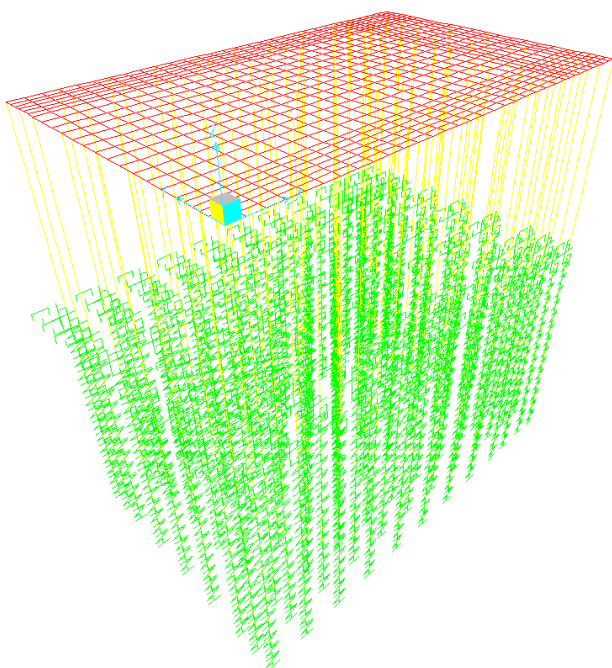


Fig. 4 The 3D finite element model used in SAP2000 v.17

2.2.1 Environmental loads

The environmental loads include current loads, wave loads and wind loads as follows:

Current Force

The drag force is given by Eq. (1) (API, 2000, Chandrasekaran 2015):

$$F_D = C_d \frac{\rho}{2} A U^2 \tag{1}$$

where F_D is the drag force (KN), C_d is the drag coefficient, ρ is the water density (t/m^3), A is the cross section (m^2) and U is the current velocity, with value 0.1-2.3m/sec (Sutcliffe and Parks 1999). This force acts on the part of piles between the water level and bed level.

Wave forces

The regular wave theories are used to calculate the forces on fixed offshore platform, illustrated in Fig. 5, and based on the three parameters of water depth (d), wave height (H) and wave period (T).

The total force is calculated by using Morison's equation, which decomposes the total force into an inertia component and a drag component (API, 2000; Chandrasekaran 2015)

$$F = \rho C_m V \frac{du}{dt} + \frac{1}{2} \rho C_d A u |u| \tag{2}$$

where F is the total force on the platform, C_m is the inertia coefficient, u is the current velocity, $\frac{du}{dt}$ is the current acceleration, and is the V object volume. This force acts on piles at water level.

Wind forces

The wind pressure as recommended by the Egyptian Code for the calculation of loads and forces ECP-201 (2008) and by API (2000) is as follows

$$q = 0.5 \rho V^2 C_t C_s \tag{3}$$

where q is the total wind pressure (KN/m^2), V is the wind velocity, ρ is the air density ($1.25 t/m^3$), C_t is the topographic factor (1.00), and C_s is the shape structure factor.

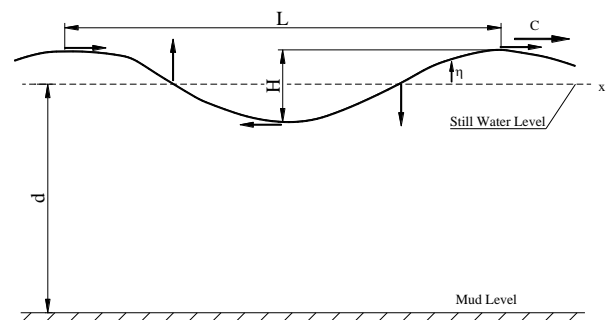


Fig. 5 Wave parameters

The wind force as recommended by the Egyptian Code for the calculation of loads and forces ECP-201 (2008) is as follows

$$F = 0.0437 C_s A_p U_{10}^2 \quad (4)$$

where F is the wind force in KN, C_s is the shape structure factor, A_p is the cross section (m^2), U_{10} is the wind velocity (Km/hr). This force acts on the part of piles over the water level and an equivalent wind force from the steel frame on the platform.

2.2.2 Earthquake loads

In this study, a materially nonlinear earthquake response spectrum analysis was performed on this riverine platform subjected to earthquake and environmental loads. This study provides a very important case to design safe piles to satisfy the requirements of the safety of the platform when it is designed with the applied earthquake and environmental loads which affect the structure in its life age.

The big projects are designed to satisfy the earthquake and environmental loads that may be subjected to in their lifetime. The most influential loads can the structures subjected to, are the earthquake loads that can make the structure collapse easily especially the connections between different kinds of elements (piles and platform). The effect of earthquake was taken into consideration in addition to the environmental loads acting on the platform, so that the actual design for such structure will study, the combination between different kinds of loads (except wind load since the earthquake effect will be taken into consideration) for the maximum effect will study to show if that structure will resist loads subjected to or not.

The earthquake is described in the Egyptian code ECP-201 (2008, 2011) by the elastic ground acceleration response spectrum $S_e(T)$, denoted as the “elastic response spectrum”. The shape of the horizontal elastic response spectrum in ECP-201 is as presented in Fig. 6.

The response spectral shape is composed by four branches:

- Very low period branch, from peak ground acceleration to the constant acceleration branch
- Constant acceleration
- Constant velocity
- Constant displacement.

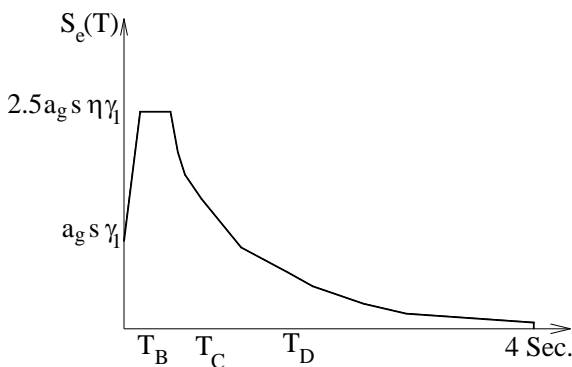


Fig. 6 Elastic response spectrum

Table 2 Values of parameters used in response spectrum analysis

Subsoil Class	S	T _B	T _C	T _D
B	1.35	0.05	0.25	1.2

The equations used for the calculation of the elastic response spectrum are

$$0 \leq T \leq T_B: \quad S_e(T) = a_g \gamma_I S \left[1 + \frac{T}{T_B} (2.5 \eta - 1) \right] \quad (5)$$

$$T_B \leq T \leq T_C: \quad S_e(T) = (2.5 a_g \gamma_I S \eta) \quad (6)$$

$$T_C \leq T \leq T_D: \quad S_e(T) = \left(2.5 a_g \gamma_I S \eta \left[\frac{T_C}{T} \right] \right) \quad (7)$$

$$T_D \leq T \leq 4 s: \quad S_e(T) = \left(2.5 a_g \gamma_I S \eta \left[\frac{T_C T_D}{T^2} \right] \right) \quad (8)$$

where

$S_e(T)$	Elastic Horizontal Response Spectrum
T	Vibration Period Time
a_g	Ground Acceleration
T_B, T_C, T_D	Limits depending on the soil type
T_B, T_C	Constant acceleration limits for elastic response spectrum
T_D	Specific value where starts constant displacement
γ_I	Importance Factor
η	Correction Damping factor (depending on the type of structure)
S	Soil Factor

In this study, we have: $a_g = 0.2g$ (Zone No. 2), $\gamma_I = 1.4$, $\eta = 1$ (reinforced concrete), Subsoil class: B. The values of parameters used in the response spectrum analysis are as shown in Table 2.

2.3 Design of piles for skin friction and bearing

In this study, the piles supporting the platform are considered as combined skin friction and bearing pile type (Mosher and Dawkins 2000, NAVFAC, 1986).

The following equations explain the capacity of the pile for both types, i.e. bearing (tip) and skin friction (side).

The ultimate tip resistance (bearing capacity of the end) Q_{tip} of the pile is represented by Eq. (9) as follow

$$Q_{tip} = A_{tip} \cdot q_{ult} = A_{tip} \cdot (N_q \cdot \sigma_v + N_c) \quad (9)$$

where:

A_{tip} is the area of pile tip;

q_{ult} is the ultimate end-bearing pressure;

σ_v is the vertical stress in soil (overburden pressure);

N_q is the bearing factor for cohesionless soils (it is a

function of friction);

N_c is the bearing factor of cohesive soil (it is a function of depth/width).

The ultimate skin friction (side resistance) participation Q_{side} in the pile capacity for friction pile is calculated by Eq. (10) as follows

$$Q_{side} = \sum \sigma_f O_i \Delta l = \sum (\sigma_0 + C_a) O_i \Delta l \quad (10)$$

where:

σ_f is the skin friction (side resistance);

C_a is the adhesion of cohesive soil;

O_i is the perimeter of pile section;

Δl is the segment of pile;

σ_0 is the skin friction of cohesionless soil, calculated as follows:

$$\sigma_0 = \sigma_h \tan \delta = K_{down} \cdot \sigma_v \cdot \tan \delta$$

where:

$$K_{down} = \sigma_h / \sigma_v$$

σ_v is the vertical stress in soil;

σ_h is the horizontal stress in soil;

K_{down} is the ratio of vertical and horizontal stress in soil;

δ is the skin friction between soil and pile (it is a function of pile skin materials);

$$C_a = K_c \cdot K_a \cdot C$$

where:

C is the shear strength of cohesive soil (cohesion);

K_c is the adhesion factor;

K_a is the adhesion ratio, C_a/C (it is a function of C).

The full ultimate downward capacity of the pile is calculated from the following Eq. (11)

$$Q_U = Q_{tip} + Q_{side} \quad (11)$$

where:

Q_U is the Ultimate downward capacity;

Q_{tip} is the Ultimate tip resistance (end-bearing capacity);

Q_{side} is the Ultimate side resistance (skin friction capacity).

2.4 Soil pile interaction

The stiffness and dashpot coefficients proposed by Roesset and Angelides (1980), Gazetas and Dobry (1984), Gazetas and Makris (1991) and Makris and Gazetas (1992) are used in this study:

Eq. (12) represents the stiffness of soil in horizontal (x, or y) direction.

$$k_x \approx 1.2E_s \quad (12)$$

Eq. (13) represents the damping of soil in horizontal (x, or y) direction.

$$c_x \approx 6a_0^{-4} \rho_s V_s d + 2\beta_s \frac{k_x}{\omega} \quad (13)$$

where E_s , V_s , β_s and ρ_s are Young's modulus, shear wave velocity, damping ratio and mass density of the supporting soil, respectively and a_0 is a dimensionless frequency

parameter defined as $a_0 = \frac{\omega d}{V_s}$.

Eq. (14) represents the stiffness of soil in vertical (z) direction.

$$k_z \approx 0.6E_s \left(1 + \frac{1}{2}\sqrt{a_0}\right) \quad (14)$$

Eq. (15) represents the damping of soil in vertical (z) direction.

$$c_z \approx a_0^{-4} \rho_s V_s d + 2\beta_s \frac{k_z}{\omega} \quad (15)$$

2.5. Soil layers of River Bed

Characterization of the soil under the bed level of the Nile River and a description of each soil layer can be found, e.g., in Warner *et al.* (1984) as shown in Table 3.

Three layers of soils under bed level were taken, through which the piles of the platform pass. Table 4 represents the herein used three river bed soil layers. These layers were transformed to 3D soil elements (springs and dashpots) arranged at all over the length of the piles from bed level until the end of the piles. Especially from bed level until 2 m under bed level (i.e., bed: -2 m), the soil is the same as that of Layer (1) in Table 4 and this depth is represented as two spring-gap elements (at 1 m under bed level, one in x direction and one in y direction) between each pile and the soil to account for the gap that may occur between each pile and the soil due to the lateral load actions, where the gap distance equals zero and the stiffness of the spring equals $k_x = k_y$ of Layer (1) in Table 4. Additionally, from 2 m to 14 m under the bed level (i.e., -2 m : -14 m), the three layers of soil (which the piles of the platform pass through) were modeled as soil springs in three-dimensions arranged all over the length of the piles until the end of the piles.

Table 3 Classification of soil under bed level of Nile River

Depth (m)	Classification
Bed : -1.50	Clay
-1.5 : -3	Clayey sand / Fine sand
-3 : -8	Clay/interbedded silty sand
-8 : -14	Sand/Clay
-14 : -15	Fine sand
-15 : -20	Medium sand
-20 : -26	Sand/gravel
-26 : -34	Coarse sand/large gravel
-34 : -45	Fine sand
More than -45	Bedrock

Table 4 The three soil layers

Layer	Depth (m)	Description
Layer (1)	-2:-4	Medium
Layer (2)	-4:-8	Stiff
Layer (3)	-8:-14	Very stiff

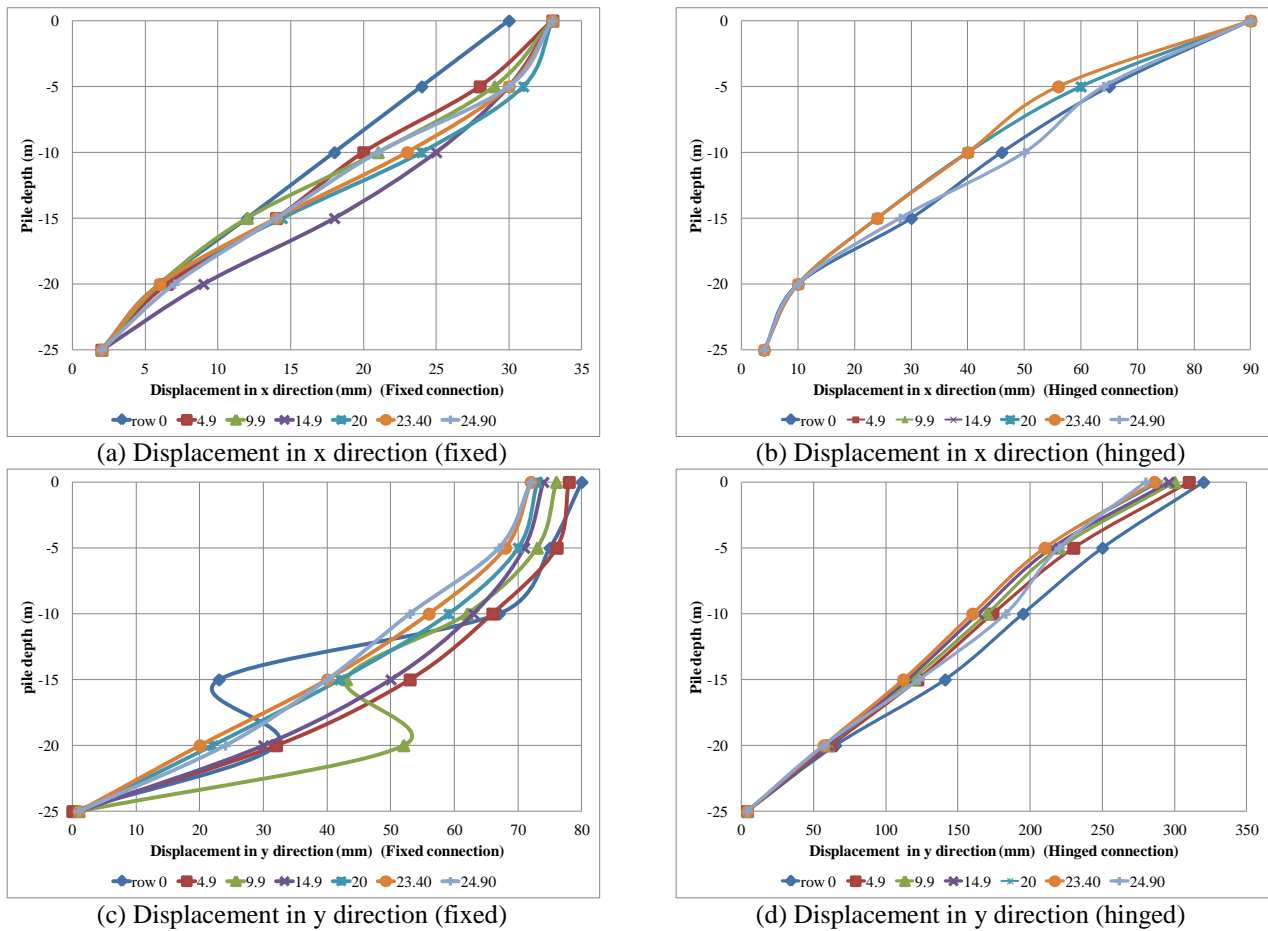


Fig. 7 Displacements of the piles in x and y directions for fixed and hinged connection between the piles and the platform

3. Results and discussion

The riverine platform constructed in the Nile River was analyzed under different loading conditions to check its ability to withstand the earthquake and environmental loads that may be exposed to. Materially nonlinear response spectrum analysis was performed on the platform and the connected piles (in fixed and hinged connection cases), the materially nonlinear properties of soil were taken into consideration and the SAP2000 v.17 software was used to analyze the model of platform and piles.

Fig. 7 shows the maximum displacements in the x and y directions with fixed and hinged pile connection for the whole depth of the piles in different distances in the platform, namely for the rows of piles with $x = 0., 4.9, 9.9, 14.9, 20., 23.4$ and 24.9 m (see Fig. 2(a)). Fig. 7(a) shows the displacements of the piles in x direction for fixed connection between the piles and the platform, where the displacement values of each row of piles are close, the maximum displacements occur at the top of the piles and the displacements reduce with increasing depth of the piles; at depth -11 m no significant effect of the soil was observed due to the interaction of the piles and the river bed, but the displacements reduced gradually by a constant ratio. Fig. 7(b) represents the displacements of the piles in x direction with hinged connections between the piles and the platform,

the displacements are bigger than the corresponding values in the fixed connection case, and the values of the displacements of each row of piles appear to be closer than the fixed case. At depth -11 m no significant change appeared in displacements, but also the values decreased gradually with a ratio of 2.7% which is greater than the corresponding ratio in fixed case (1.32%).

Fig. 7(c) shows the displacements of the piles in y direction with fixed connections, where for the top 5 m of the piles the displacements are almost constant and gradually decrease with a constant ratio of 3%. Fig. 7(d) represents the displacements of the piles in y direction with hinged connections, where the displacements of the piles for each row of piles are close with a decrease ratio equal to 12.8%, and the displacements of the piles in the hinged case are bigger than the corresponding values in the fixed connection case.

Fig. 8 shows the maximum shear forces in x and y directions in the piles with fixed and hinged platform connection at different distances in the platform, namely for the rows of piles with $x = 0., 4.9, 9.9, 14.9, 20., 23.4$ and 24.9 m (see Fig. 2(a)). Fig. 8(a) shows the shear forces in x direction in the piles with fixed connection between the piles and the platform, where the shear forces in piles increase (except for piles at distances zero and 4.9 m which initially decrease and afterwards increase) until about the

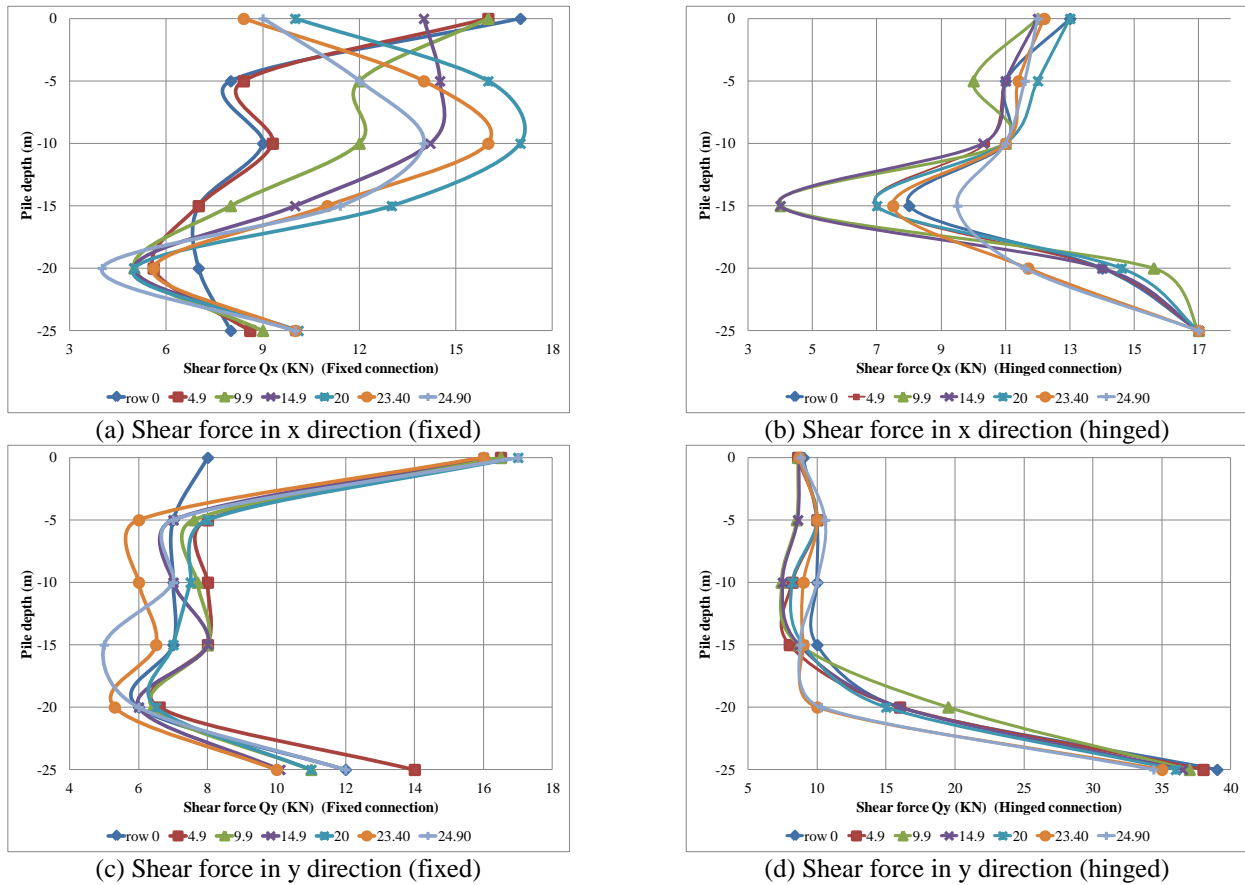
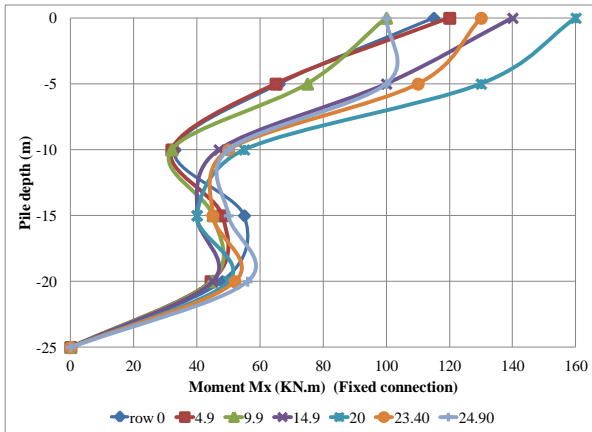


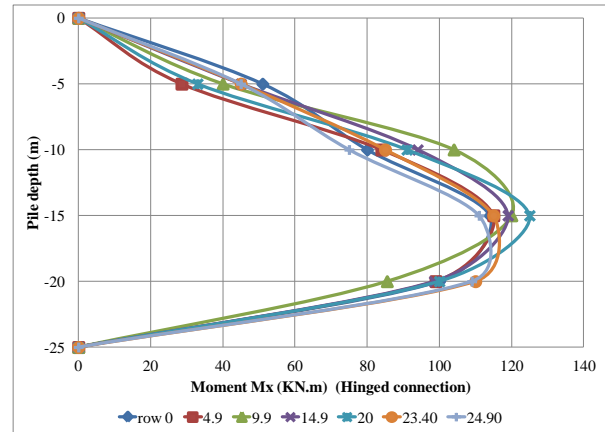
Fig. 8 Shear forces in piles with fixed and hinged connection between the piles and the platform

bed level depth (-11 m) because of the pounding between soil and piles, after that the shear forces decrease until the depth -20 m (about equal to half the embedded length of the pile) and then the shear forces increase in the last 5 m depth of the piles until the end of the piles. Fig. 8(b) shows the shear forces in the x direction in the piles with hinged connection which are nearly similar at the bed level for all piles, afterwards the shear forces decrease at depth -15 m and then increase gradually until the end of the piles. From Figs. 8(a) and 8(b) it is observed that at end of the piles the shear forces in x direction with fixed connection decrease by 1.75 times more than the corresponding values in the hinged connection case, but at bed level the shear forces in the fixed case increase by 1.50 times than the corresponding values in the hinged case. Fig. 8(c) represents the shear forces in y direction in piles with fixed connection case, which have nearly constant values from depth -5 m until -20 m and the maximum shear force values are at the top and end of the piles (where shear forces at the top of the piles equals 2 times the constant shear force values and at the end of the piles equals 1.5 times the constant shear force values). Fig. 8(d) shows the shear forces in piles in y direction with hinged connection, where shear forces are nearly constant from top until depth -15 m, then increase until the end of the piles and the increase in shear forces from depth -15 m until -25 m equals to 4 times. The shear forces in the fixed case are generally decreased than the hinged case by nearly 4 times especially at end of the piles.

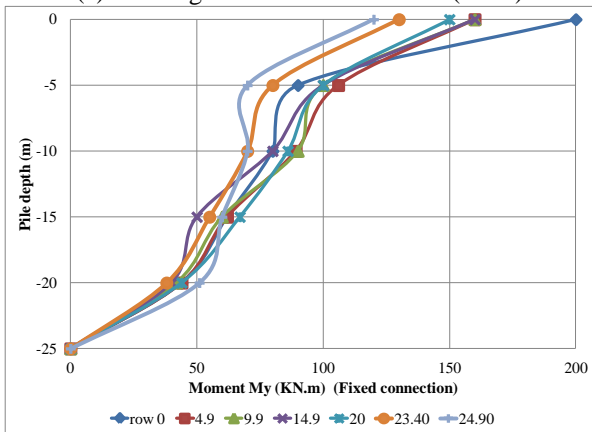
Fig. 9 represents the bending moments in x any y directions in the piles with fixed and hinged platform connection at different distances of the platform, namely for the rows of piles with $x = 0., 4.9, 9.9, 14.9, 20., 23.4$ and 24.9 m (see Fig. 2(a)). Fig. 9(a) shows the bending moments in x direction in the piles with fixed connection between the piles and the platform, where the maximum bending moments occur at the top of the piles, bending moments are nearly constant from the bed level depth (-11 m) until depth -20 m, and the from depth -20 m the bending moments decrease sharply to zero. Fig. 9(b) shows the bending moments in x direction in the piles with hinged connection, where the moments are equal to zero at the top and end of the piles, the maximum bending moments occur at depth of about -15 m then decrease. The maximum bending moments in x direction in both connection cases are of similar values but the location of these maximum bending moments are different in each case, so the location of the main reinforcement in each case must be taken into concern. Fig. 9(c) shows the bending moments in y direction in the piles with fixed connection case, where the maximum bending moments occur at top of the piles, decrease until the bed level (-11 m) and then again decrease gradually from depth of -20 m until the end of the piles. Fig. 9iv shows the bending moments in y direction in the piles with hinged connection, where the maximum bending moments occur at depth of -15 m and then decrease gradually until the end of the piles. The maximum bending



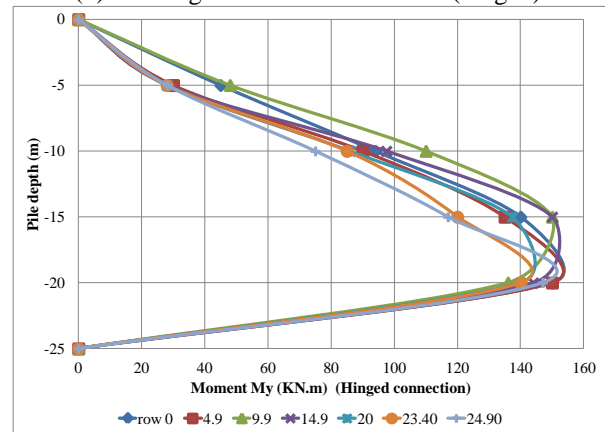
(a) Bending moment in x direction (fixed)



(b) Bending moment in x direction (hinged)

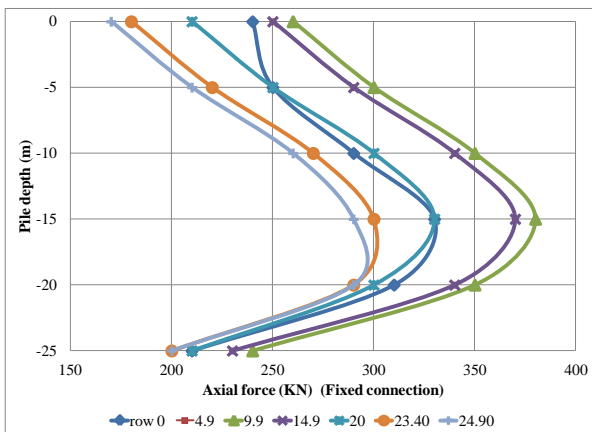


(c) Bending moment in y direction (fixed)

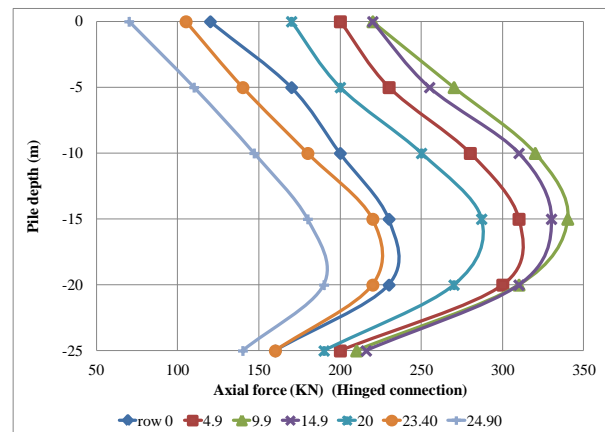


(d) Bending moment in y direction (hinged)

Fig. 9 Bending moments in piles with fixed and hinged connection between the piles and the platform



(a) Fixed connection



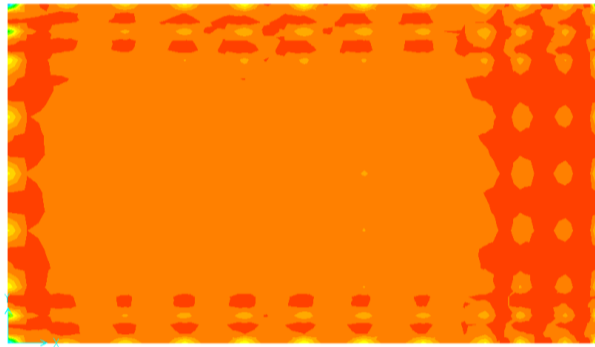
(b) Hinged connection

Fig. 10 Axial forces in the piles with fixed and hinged connection between the piles and the platform

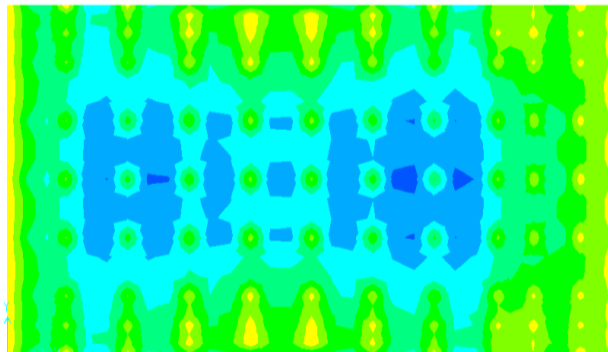
moments in y direction in each connection case are of similar values but the location of these maximum bending moments are different in each case.

Fig. 10 represents the axial forces in the piles with fixed and hinged platform connection cases at different distances of the platform, namely for the rows of piles with $x = 0.$, 4.9, 9.9, 14.9, 20., 23.4 and 24.9 m (see Fig. 2(a)). Fig.

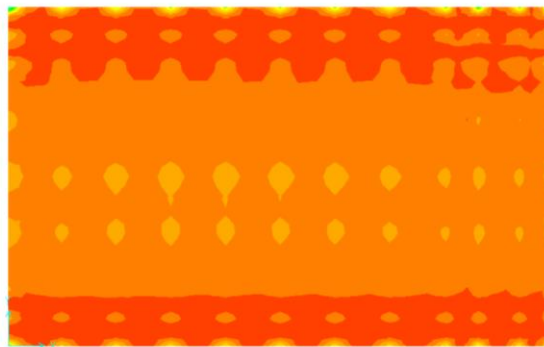
10(a) represents the axial forces in the piles with fixed connection, where the values of the axial forces in the piles are diverse at different distances of the platform with maximum value equal to 375 KN which occur at about depth of -15 m and then the axial forces are gradually decreasing until specific values at the end of the piles (range from about 200 to 240 KN). Fig. 10(b) represents the axial



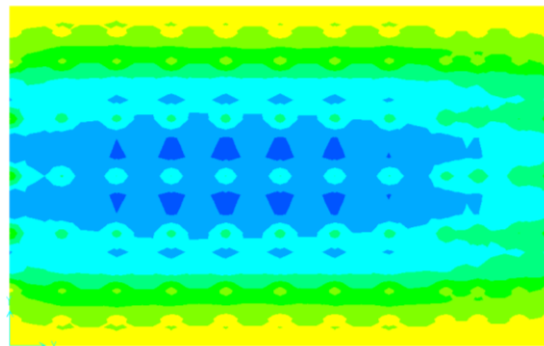
(a) Stress in x direction, maximum=88396.191 KN/m² (fixed connection)



(b) Stress in x direction, maximum=15563.459 KN/m² (hinged connection)



(c) Stress in y direction, maximum=111083.41 KN/m² (fixed connection)



(d) Stress in y direction, maximum=25332.834 KN/m² (hinged connection)

Fig. 11 Stresses (KN/m²) in the platform with different piles platform connections conditions

forces in the piles with hinged connections, where the axial force values are diverse for piles at different distances of the platform and the maximum axial force (340 KN) in the piles occurs at depth of about -15 m and then axial forces gradually decrease until specific values at the end of the piles (range from about 140 to 220 KN).

Fig. 11 depicts the stresses in the platform in x and y directions. Fig. 11(a) depicts the stress in x direction with fixed connection, where the maximum stress is equal to 88396.191 KN/m². Fig. 11(b) depicts the stress in x direction with hinged connection where the maximum stress is equal to 15563.459 KN/m².

Fig. 11(c) depicts the stress in y direction with fixed connection, where the maximum stress is equal to 111083.41 KN/m². Fig. 11(d) depicts the stress in y direction with hinged connection, where the maximum stress is equal to 25332.834 KN/m².

4. Conclusions

A realistic 3D-FEM structural model was developed and a materially nonlinear earthquake response spectrum analysis was performed for an existing pile-supported riverine platform incorporating soil-pile interaction in order to study its structural response under earthquake and environmental loads. The environmental loads acting on this platform were wind, water waves, and water current loads. The pile response in terms of displacements, shear forces, bending moments, and normal forces were obtained assuming a fixed or hinged connection between the piles and the reinforced concrete platform. The interaction between the transfer plate and the piles supporting the platform was investigated. Transfer plate structures have the ability to redistribute the loads from the superstructure above to piles group below, to provide safe transits of loads to piles group and thus to the soil, without failure of soil or structural elements. The distribution of piles affects the distribution of stress on both soil and platform. The seismic soil-pile-structure interaction increases lateral displacement, which may shift the performance level of the structure from life safe to collapse level.

A fixed connection between the piles and the platform is better in the design of the piles and the prospect of piles collapse is low while a hinged connection makes the prospect of damage high because of the larger displacements. The piles suffer from displacement failure than force failure. A fixed connection between the piles and the platform is the most demanding case in the design of the platform slab (transfer plate) because of the high stress values developed.

References

Abdel-Mohti, A. and Khodair, Y. (2014), "Analytical investigation of pile-soil interaction in sand under axial and lateral loads", *Int. J. Adv. Struct. Eng.*, **6**(54), 1–16.
 Abu Seif, E.S.S. and El-Shater, A.A. (2010), "Engineering aspects and associated problems of flood plain deposits in Sohag Governorate, Upper Egypt", *J. Am. Sci.*, **6**, 1614-1623.

API (American Petroleum Institute) (2000), *API Recommended Practice 2A-WSD (RP 2A-WSD), Recommended Practice for Planning, Designing and Constructing Fixed Offshore Platforms—Working Stress Design*, (21st edition), American Petroleum Institute (API), Washington, DC, USA.
 Asgarian, B., Shokrgozar, H.R., Shahcheraghi, D. and Ghasemzadeh, H. (2012), "Effect of soil pile structure interaction on dynamic characteristics of jacket type offshore platforms", *Coupled Syst. Mech.*, **1**(4), 381-395.
 Chandrasekaran, S. (2015), *Dynamic Analysis and Design of Offshore Structures*, (1st Edition), Springer India, New Delhi, India.
 Chatterjee, K., Choudhury, D. and Poulos, H.G. (2015), "Seismic analysis of laterally loaded pile under influence of vertical loading using finite element method", *Comput. Geotech.*, **67**, 172-186.
 Chau, K.T., Shen, C.Y. and Guo, X. (2009), "Nonlinear seismic soil-pile-structure interactions: Shaking table tests and FEM analyses", *Soil Dyn. Earthq. Eng.*, **29**(2), 300-310.
 Cheng, J. and Liu, X.-I. (2012), "Reliability analysis of steel cable-stayed bridges including soil-pile interaction", *Steel Compos. Struct.*, **13**(2), 109-122.
 Chore, H.S. and Ingle, R.K. (2008), "Interaction Analysis of Building Frame Supported on Pile Group", *Indian Geotech. J.*, **38**, 483-501.
 Chore, H.S., Ingle, R.K. and Sawant, V.A. (2010), "Building frame-pile foundation-soil interaction analysis: A parametric study", *Interact. Multiscale Mech.*, **3**(1), 55-79.
 Dode, P.A., Chore, H.S. and Agrawal, D.K. (2014), "Interaction analysis of a building frame supported on pile groups", *Coupled Syst. Mech.*, **3**(3), 305-318.
 Durante, M.G., Di Sarno, L., Mylonakis, G., Taylor, C.A. and Simonelli, A.L. (2015), "Soil-pile-structure interaction: Experimental outcomes from shaking table tests", *Earthq. Eng. Struct. D.*, **45**, 1041-1061.
 ECP-201: Egyptian Code of Practice for loading (2008), *Egyptian Code for Calculating Loads and Forces in Structural Work and Masonry (ECP-201)*, Housing and Building National Research Center, Ministry of Housing, Utilities and Urban Planning, Cairo, Egypt.
 Elnashai, A.S. and Di Sarno, L. (2015), *Fundamentals of Earthquake Engineering: From Source to Fragility*, (2nd Ed.), John Wiley & Sons, Ltd., Chichester, UK.
 Gazetas, G. and Dobry, R. (1984), "Horizontal response of piles in layered soils", *J. Geotechn. Eng. - ASCE*, **110**(1), 20-40.
 Gazetas, G. and Makris, N. (1991), "Dynamic pile-soil-pile interaction. Part I: analysis of axial vibration", *Earthq. Eng. Struct. D.*, **20**(2), 115-132.
 Hamilton, M. (2014), *Pile-Soil Interaction in Unsaturated Soil Conditions; Senior Honors Thesis in Partial Fulfillment of the Requirements for Honors in Civil Engineering*, University of New Hampshire, Durham, NH, USA.
 Hussien, M.N., Tobita, T. and Iai, S. (2010), "Experimental and FE analysis of seismic soil-pile-superstructure interaction in sand", *Ann. Disaster Prev. Res. Inst. B*, **53**, 299-306.
 Kaynia, A.M. (2012), "Dynamic response of pile foundations with flexible slabs", *Earthq. Struct.*, **3**, 495–506.
 Kaynia, A.M. and Andersen, K.H. (2015), "Development of nonlinear foundation springs for dynamic analysis of platforms", *Proceedings of the Frontiers in Offshore Geotechnics III-3rd International Symposium on Frontiers in Offshore Geotechnics (ISFOG 2015)*, Oslo, Norway, 10–12 June; Meyer, V. (Ed.), CRC Press/Balkema-Taylor & Francis Group, Leiden, The Netherlands.
 Kaynia, A.M., Norén-Cosgriff, K., Andersen, K.H. and Tuen, K.A. (2015), "Nonlinear foundation spring and calibration using measured dynamic response of structure", *Proceedings of the*

- 34th International Conference on Ocean, Offshore and Arctic Engineering, OMAE2015, St. John's, NL, Canada, 31 May–5 June; ASME, New York, NY, USA.
- Kim, S.B., Yoon, G.L., Yi, J.H. and Lee, J.H. (2015), "Reliability analysis of laterally loaded piles for an offshore wind turbine support structure using response surface methodology", *Wind Struct.*, **21**(6), 597-607.
- Lysmer, J. and Kuhlemeyer, R.L. (1969), "Finite dynamic model for Infinite media", *J. Eng. Mech. Div.-ASCE*, **95**(4), 859-878.
- Makris, N. and Gazetas, G. (1992), "Dynamic pile-soil-pile interaction. Part II: lateral and seismic response", *Earthq. Eng. Struct. D.*, **21**(2), 145-162.
- Mandal, B., Roy, R. and Dutta, S.C. (2012), "Lateral capacity of piles in layered soil: A simple approach", *Struct. Eng. Mech.*, **44**(5), 571-584.
- Mehndiratta, S., Sawant, V.A. and Samadhiya, N.K. (2014), "Nonlinear dynamic analysis of laterally loaded pile", *Struct. Eng. Mech.*, **49**(4), 479-489.
- Mosher, R.L. and Dawkins, W.P. (2000), *Theoretical Manual for Pile Foundations*, Report ERDC/ITL TR-00-5, U.S. Army Corps of Engineers, Engineer Research and Development Center, Washington, DC, USA.
- NAVFAC (Naval Facilities Engineering Command) (1986), *Foundations and Earth Structures-Naval Facilities Engineering Command Design Manual 7.02 (NAVFAC DM 7.02)*, Naval Facilities Engineering Command (NAVFAC), Alexandria, VA, USA.
- Newmark, N.M. and Rosenblueth, E. (1971), *Fundamentals of Earthquake Engineering*, Prentice-Hall, Englewood Cliffs, NJ, USA.
- Ravi Kumar Reddy, C. and Gunneswara Rao, T.D. (2011), "Experimental study of a modeled building frame supported by pile groups embedded in cohesionless soil", *Interact. Multiscale Mech.*, **4**(4), 321-336.
- Razavi, S.A., Fakher, A. and Mirghaderi, S.R. (2007), "An Insight into the Bad Reputation of Batter Piles in Seismic Performance of Wharves", *Proceedings of the 4th International Conference on Earthquake Geotechnical Engineering*, Thessaloniki, Greece, 25–28 June; Pitilakis, K.D. (Ed.), Springer, Dordrecht, Germany.
- Roesset, J.M. and Angelides, D. (1980), "Dynamic Stiffness of Piles", *Numerical Methods in Offshore Piling*, Institution of Civil Engineers, 75-80.
- SAP2000[®] Version 17 (2015), *Integrated Software for Structural Analysis and Design*, Computers and Structures, Inc., Walnut Creek, CA & New York, NY, USA.
- Sutcliffe, J.V. and Parks, Y.P. (1999), *The Hydrology of the Nile*, Institute of Hydrology, International Association of Hydrological Sciences (IAHS) Special Publication No. 5, IAHS Press, Wallingford, UK.
- Tallavó, F., Martinez, M.E. and Ewins, D.J. (1995), "Experimental evaluation of vibrations in an operating offshore platform", *Proceedings of the 13th International Modal Analysis Conference (IMAC XIII)*, Nashville, TN, USA, 13–16 February; Society for Experimental Mechanics Inc., Bethel, CT, USA, pp. 1847–1852.
- Ukritchon, B., Faustino, J.C. and Keawsawasvong, S. (2016), "Numerical investigations of pile load distribution in pile group foundation subjected to vertical load and large moment", *Geomech. Eng.*, **10**(5), 577–598.
- Warner, J.W., Gates, T.K., Fahim, W., Ibrahim, M., Awad, M. and Ley, T.W. (1984), *Hydraulic Conductivity and Vertical Leakage in the Clay Silt Layer of the Nile Alluvium in Egypt*, Technical Report No. 60; Egypt Water Use and Management Project, Water Distribution Research Institute, Water Research Center, Ministry of Irrigation, Government of Egypt, Cairo, Egypt.
- Yi, J.H., Kim, S.B., Yoon, G.L. and Andersen, L.V. (2015), "Natural frequency of bottom-fixed offshore wind turbines considering pile-soil-interaction with material uncertainties and scouring depth", *Wind Struct.*, **21**(6), 625–639.

CC